KECK Geology Consortium
Learning Science Through Research
Published by Keck Geology Consortium
Short Contributions
30th Annual Symposium Volume
29th April, 2017
ISBN: 1528-7491

THE TECTONIC EVOLUTION OF A DEEPLY EXHUMED ARC SECTION: A PETROLOGICAL STUDY OF THE EMPLACEMENT OF THE SIERRA DE SALINAS SCHIST

VERONICA PADILLA VRIESMAN, Colgate University
Research Advisor: Martin Wong

INTRODUCTION

The California coast possesses a diverse array of subduction-related geologic features that help to constrain the region's tectonic evolution during the Jurassic and the early Tertiary. The much-studied Sevier and Laramide orogenic events reflect fluctuating angles of subduction, which makes California an attractive location for studying the implications of flat-slab subduction. In particular, Big Sur and its associated mountain ranges provide a source of great structural complexity and petrologic diversity. Sierra de Salinas—a schist body dating back to the late Cretaceous—is located approximately 50 km to the northeast of Big Sur and serves as the focal point of this particular study. It is an ideal environment for examining the possible tectonic phenomenon known as "cold relamination", or progressive underplating. The inverted metamorphic field gradient and varying manifestations of deformation (both coaxial and non-coaxial within the same schist body) point to cold relamination as the driving mechanism of the schist's emplacement.

Sierra de Salinas remains understudied and poorly understood, likely due to the ambiguity surrounding its geographical and geological origins. It is part of a belt of schist exposures that likely represents the accretionary wedge underplated below the North American continent, which explains why progressive underplating is a reasonable explanation for the petrogenesis of these large schist bodies. Associated schist exposures include the Pelona, Orocopia, and Rand schists, all with present-day locations in southern and central California (Ducea et al., 2005).

This study aims to place constraints on emplacement mechanisms of the schist of Sierra de Salinas by relying on microstructural and crystallographic preferred orientation (CPO) data, gathered via petrographic observation and EBSD analyses. This work will hopefully provide some insight into the processes of underplating and crustal deformation, which will hold the potential to address uncertainty in other cases of deeply exhumed arc sections and metamorphosed accretionary wedges.

GEOLOGIC SETTING

Sierra de Salinas is a composite terrane located in the Coast Range Mountains of central California. The Coast Ranges are thought to be a product of subduction and large-scale displacement along the various fault systems in the area, including the San Andreas fault. The Salinia terrane formed beneath southern California and western Arizona, where it is exposed along small detachment faults (Cheadle, et al. 1986). The terrane was then transported to central California by ~330 km of right-lateral slip along the San Andreas fault to its present location (Kidder et al., 2006).

The petrogenesis of the schist of Sierra de Salinas is attributed to the subduction of a deep-sea trench filled with accretionary sediments. The trench became submerged below North America as the Laramide subduction event occurred during the Late Cretaceous. During the Laramide orogeny, the Farallon plate began to subduct at an anomalously shallow angle, a phenomenon known as flat-slab subduction. The magmatic arc served as a source of accretionary sediments, which were quickly deposited into the

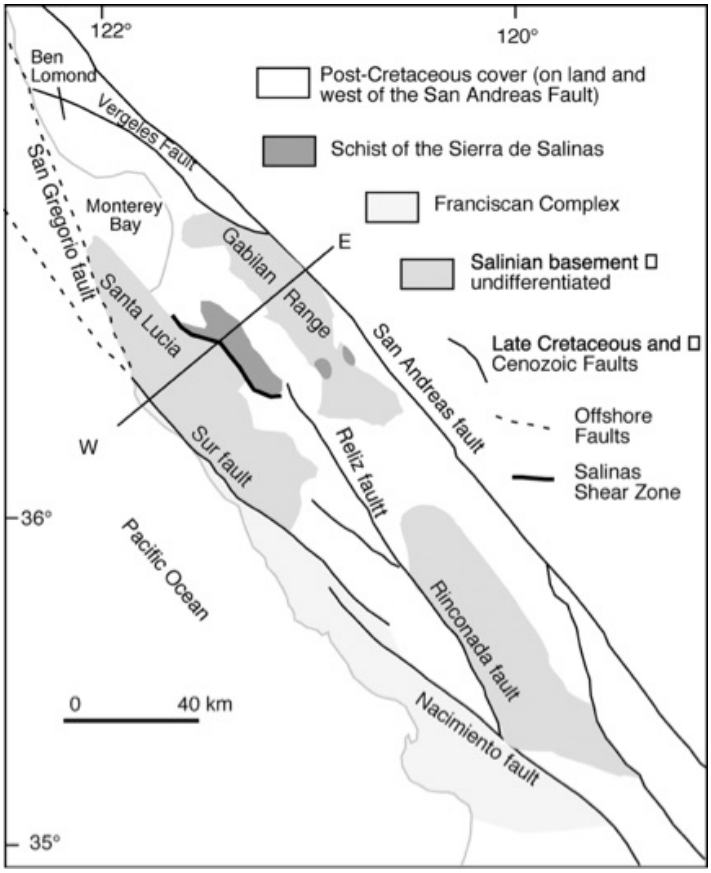

Figure 1. Map of the study area, showing the Sierra de Salinas schist bounded by various brittle faults. Courtesy of Ducea et al, 2009.

trench. As the trench itself subducted, these sediments were underplated and subsequently metamorphosed below the Californian arc (Saleeby, 2003).

Sierra de Salinas is dominated by metagraywacke, or biotite-rich quartzose schist. All associated schists are results of the underplating of forearc sediments below the Californian arc from 90-50 Ma during shallow subduction of the Farallon plate, but Sierra de Salinas possesses the main surface exposure of the schist (Ducea et al., 2009). The Rinconada-Reliz fault imposed ~44 km of right-lateral slip during the Late Tertiary (Dibblee, 1976), which represents significant displacement but is not nearly as extensive as the large-scale terrane migration caused by the San Andreas fault, which serves as the eastern border of Sierra de Salinas (see Fig. 1). The schist is also bounded to the west by the ductile Sur-Nacimiento fault, which defines the Salinas shear zone. This western border separates the rest of the Salinian block from Sierra de Salinas. The Big Pine fault cuts through the southern portion of the Sierras, forming

Figure 2. A map created from Google Images showing the five sample locations in the area of study. Note that 3 samples come from the northern end of Sierra de Salinas while 2 come from the southern end.

the southernmost boundary of Sierra de Salinas (Vedder et al., 1982). The schist is juxtaposed with plutonic rocks that are analogous to the plutons of Sierra Nevada and Peninsular Range batholiths in terms of age, mineralogic composition, and isotopic signature (Kistler et al., 2001).

METHODS

Fieldwork

During fieldwork, five oriented samples were collected from varying depths of the Sierra de Salinas Mountains. The five samples have been pinpointed on the map in Figure 2. All samples were selected based on their proximity to one another as well as their respective structural depths. Samples 16SLM6, 16SLM11, and 16SLM8 represent the shallowest part of the schist body. They are most central to the shear zone, and the extent of their brittle deformation is evident even in hand sample. Schist samples were difficult to collect because of poor exposure, severe weathering, and property access restraints. The deepest part of the schist body is represented by samples 16SLM7 and 16SLM9.

Laboratory Methods

Prior to preparing thin sections, each hand sample was cut perpendicular to foliation and parallel to lineation. Since all five schist samples were severely weathered—and therefore prone to crumbling and

splintering—each billet was cured overnight in Epofix cold-setting embedding resin. This step held together the schist, which otherwise would have crumbled upon contact with the diamond blade. Using the polishing equipment at Macalester College and the colloidal silica polisher at the University of Minnesota, each thin section was polished to a thickness of 30 μm. At Colgate University, I used an optical microscope to examine mineralogic, petrologic, and microstructural trends in the thin sections.

Scanning Electron Microscopy (SEM) and Electron Backscatter Diffraction (EBSD) technology from the University of Minnesota allowed me to examine the crystallographic preferred orientations (CPO) of the schists' mineral fabrics more closely. I used the JEOL JSM-6500F field emission SEM in the Characterization Facility of Shepherd Labs to run the five samples, each with a working distance of 25.1 mm and a step size of 50 μm. Due to time constraints during my time at the University of Minnesota, I could only run each sample once. The figures produced from these EBSD sessions served as sufficient preliminary evidence, but in order to generate clearer maps and more substantial pole figures, I conducted further EBSD analysis at Colgate University using the JEOL JSM636OLV SEM with a Nordlys EBSD Detector. I decided to index only for quartz this time because of the lack of useable data provided by the biotite and feldspar. Using high magnification on an optical microscope, I searched for quartz bands, relict quartz grains, and newly recrystallized quartz and placed a small box around the area with a permanent marker. Drawing these boxes made navigation faster and the areas of interest much easier to locate once the sample was loaded into the SEM. Using low-vacuum mode and a pressure of ~30 Pa, I set the working distance to 15 and established a step size ranging from 8 to 15 μm, depending on the grain size typical of each thin section. I used Tango and Mambo, EBSD post-processing software, to obtain orientation maps and pole figures.

RESULTS

Shallow Samples (16SLM6, 16SLM11, 16SLM8)

In order of structural depth, from shallow to intermediate, the samples are ordered as 16SLM6, 16SLM8, and 16SLM11. Petrographic observations highlight the extent of brittle deformation present in these samples. In 16SLM6 in particular, the most noteworthy microstructural features include undulatory extinction and microscopic brittle deformation, as seen in Figure 3. Tiny intracrystalline cracks seem to dominate over signs of ductile deformation. There are some early signs of bulging recrystallization around larger quartz grains in select spots, but recrystallization is still not a dominant process. Feldspar grains remain intact, suggesting that this schist is a product of low temperature conditions, <400°C (Passchier and Trouw, 1996). Additionally, the cracking in the quartz grains places further constraints on the temperature since brittle deformation in quartz is dominant only at temperatures below 300°C (Passchier and Trouw, 1996). 16SLM6 pole figures exhibit a concentration of c-axes that generally lay perpendicular to the lineation and parallel to the foliation of the schist. This would be prism <a> slip, indicating non-coaxial strain at low temperatures since prisma <a> appears to be acting in concert with other systems, as seen by the cross-girdle patterns (Passchier and Trouw, 1996).

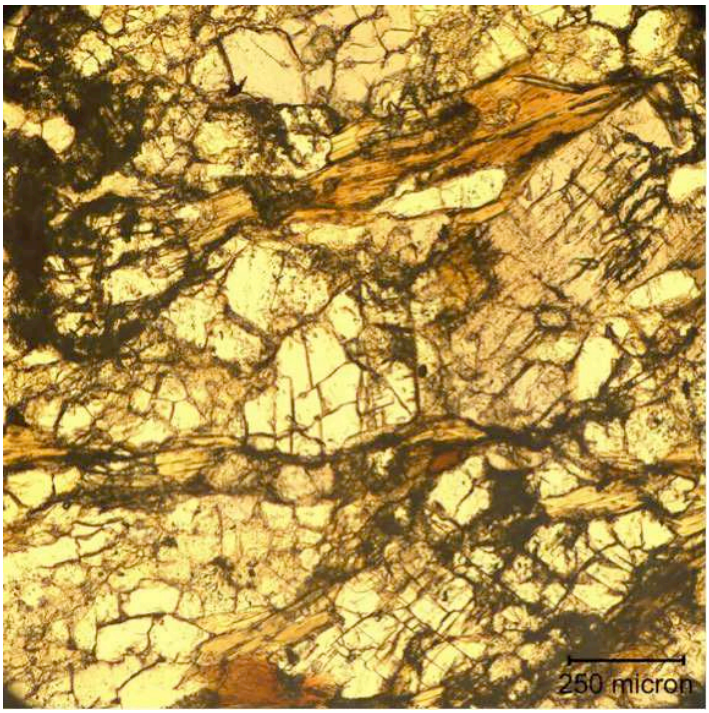

Figure 3. The microphotograph of 16SLM6 captures the small cracks in quartz grains indicative of brittle deformation. The magnification is 10x / .25 POL under plane polarized light.

The next shallowest sample, 16SLM11, generated a very poor CPO, but the concentration of c-axes seems to suggest prism <a> slip. This sample has also undergone severe ductile deformation, as seen by the splintering of biotite grains in thin section. The sample representing intermediate structural depths, 16SLM8, exhibits a weak CPO but shares a cross-girdle pattern comparable to 16SLM6, which is a weak, slightly asymmetric cross-girdle and signs of prism <a> slip. Interestingly, 16SLM8 is structurally shallower than 16SLM7, yet 16SLM8 pole figures reflect higher temperatures of deformation than do those generated by 16SLM7. In thin section, 16SLM8 displays elongate quartz grains with sweeping extinction, which are indicators of relatively low temperature deformation in 16SLM7 and 16SLM8 as well. Although these samples come from similar structural depths, they show evidence of slightly higher temperature deformation. 16SLM8 also possesses C'-type shear bands that cut obliquely through the primary foliation, which may represent a zone of increased non-coaxial flow (Passchier and Trouw, 1996). According to Passchier and Trouw, the formation of C'-type shear band cleavage is not a process that is well understood. They are typically seen in mylonitic micaschists, such as the schist of Sierra de Salinas. Their development likely takes place after ductile deformation already succeeded in generating a clear mineral preferred orientation, implying that C'-type shear bands represent late—or more recent—shear zone activity. Sub-grain boundary rotation (SGR), a function of simple shear, is the dominant deformation mechanism in 16SLM8, suggesting that it may have been subjected to slightly higher temperatures than 16SLM7, introducing the possibility of an inverted metamorphic field gradient. It is typically expected that the degree of metamorphism increases with depth, so this inversion of depth and metamorphic grade is particularly significant.

Deep Samples (16SLM7 and 16SLM9)

16SLM7 produced a CPO very similar to 16SLM6, despite the variation in structural depth. Prism <a> slip appears to be the slip system at play here, although there is also a weak cross-girdle with a right-leaning limb, suggesting a top to the right sense of shear. The pole figure could be compared to the oriented thin section to determine a top to the north sense of shear.

16SLM9—the deepest sample—represents a sharp departure from the brittle deformation that characterizes the shallower schists from the northern end of Sierra de Salinas. 16SLM9 is dominated by tiny quartz grains, likely the product of grain boundary migration recrystallization (GBM). Additionally, features of intragranular deformation are much less pronounced, further confirming GBM as the dominant regime. The lack of undulatory extinction and the replacement of unstable relict grains by newly recrystallized grains may mean that the temperature was high enough for annealing to take place, resulting in the recovery and recrystallization of quartz grains by the removal of dislocation tangles and the straightening of grain boundaries (Passchier and Trouw, 1996). EBSD results for 16SLM9 reflect a weak CPO with no clear Type I cross-girdle (Fig. 4), suggesting that plane strain can be ruled out. Roughly symmetric c-axis fabric and Type II cross-girdles are also present, indicating constrictional strain (Passchier and Trouw, 1996). See Figure 5, below, for comparison.

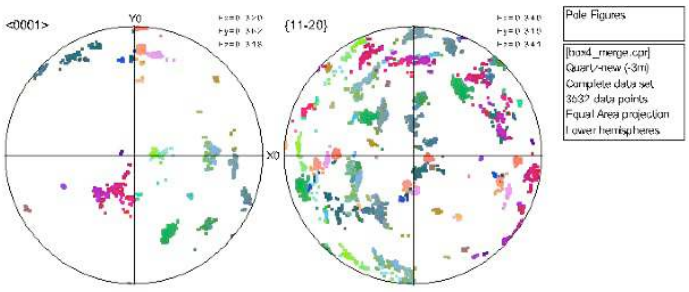

Figure 4. EBSD pole figures for 16SLM9 generated by Tango EBSD post-processing software. Note the lack of a Type I cross girdle and the extremely weak CPO.

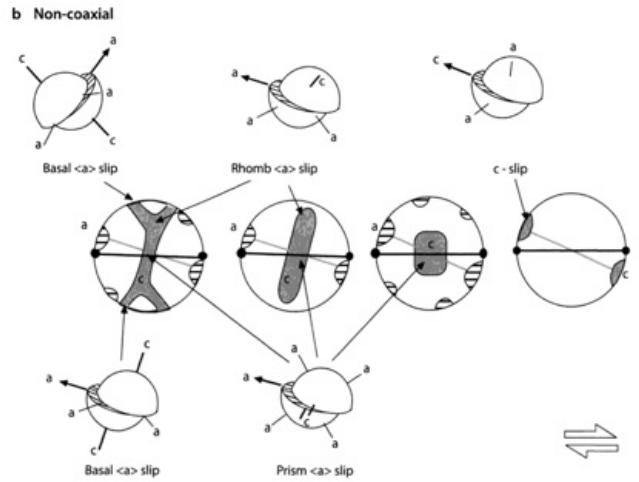

Figure 5. Modified from Passchier and Trouw, 1996. These illustrations of pole figures depict the prism <a> slip planes and c-axis patterns present in the pole figures from the Sierra de Salinas schist samples (far left, low T). Progressive non-coaxial deformation as a function of temperature, with temperature progressing from left to right.

DISCUSSION

There is evidence for an inverted metamorphic field gradient, as found previously by Kidder and Ducea, 2006. Samples 16SLM11, 16SLM7, and 16SLM8 all clearly follow this trend. 16SLM9 could also support the metamorphic inversion, although the petrographic data suggest that 16SLM9 has undergone the highest temperatures of deformation. The EBSD data, however, suggest that the deepest schist has experienced constrictional strain, while the shallower samples have undergone non-coaxial strain in a top to the north sense of shear, as shown by the kinematic indicators in thin section. Well-developed quartz CPOs in the shallower samples highlight the degree of strain that this structurally shallow schist has experienced, while structurally deeper schist produces weaker CPOs and shows signs of coaxial progressive deformation rather than non-coaxial deformation.

I propose that the schist was emplaced gradually via progressive underplating, producing both brittle and ductile deformation as schist was emplaced, then cooled, and then more was emplaced and allowed to cool. This gradual emplacement and successive underplating would explain the possible inverted metamorphic gradient as well as the switch from non-coxial to coaxial deformation as depth increases. The consistent foliation orientation, the dominance of non-coaxial strain in shallow samples and constrictional strain in deep samples, and the inconsistency between depth and temperature of deformation can be interpreted as mechanisms of underplating, or a process now referred to as “cold relamination” (Behn et al., 2011). While this study proposes a possible scenario for the formation and exhumation of the Salinian arc, further study is required to reach any sense of certainty.

ACKNOLWEDGMENTS

I would like to thank the Keck Consortium and Alan Chapman and Sarah Brownlee for extending this opportunity to me. This summer research experience was made possible by generous funding from the Keck Geology Consortium, the National Science Foundation, and ExxonMobil. I am also very grateful to my Colgate thesis advisor, Martin Wong, for his patience and problem-solving abilities. Additionally, I would like to thank my academic advisor, Connie Soja, who is the reason I chose to study geology. Lastly, I must thank my parents, Dolores and Robert, for showing me the beauty of learning and teaching, and for being consistently delighted by my passion for geology.

REFERENCES

Barth, A.P., Wooden, J.L., Grove, M., Jacobson, C.E. and Pedrick, J.N., 2003. U□Pb zircon geochronology of rocks in the Salinas Valley region of California. A reevaluation of the crustal structure and origin of the Salinian block: Geology, 31: 517–520.

Behn, M.D., Kelemen, P.B., Hirth, G., Hacker, B.R., Massonne, H.-J., 2011. Diapirs as the source of the sediment signature in arc lavas: Nature 4, 641–646.

Chapman, A.D., S. Kidder, Saleeby, J.B., and M.N. Ducea, 2010. Role of extrusion of the Rand and Sierra de Salinas schists in Late Cretaceous extension and rotation of the southern Sierra Nevada and vicinity: Tectonics, 29.

Cheadle, M.J., Czuchra, B.L., Byrne, T., Ando, C.J., Oliver, J.E., Brown, L.D.,

Kaufman, S., Malin, P.E., and Phinney, R.A., 1986. The deep crustal structure of the Mojave Desert,

California, from Cocorp seismic reflection data: Tectonics, 5(2), 293–320.
Dibblee, T.W. Jr., 1976. The Rinconada and related faults in the southern Coast Ranges, California, and their tectonic significance, US Geological Survey.
Ducea, M.N., Kidder, S., Chesley, J.T., and Saleeby, J.B., 2009. Tectonic underplating of trench sediments beneath magmatic arcs: the central California example: International Geology Review, Volume 51, Issue 1, 1-26.
Ducea, M.N., Kidder, S., Chesley, J.T., 2005. Salinia: A Crustal Cross Section Through a Shallow Subduction Zone Exposing the Subduction Megathrust: AAPG from Geological Society of America, Vol. 37, No. 4, 52.
Kidder, S., Ducea, M.N., 2006. High temperatures and inverted metamorphism in the schist of Sierra de Salinas, California: Earth and Planetary Science Letters, Volume 241, Issues 3–4, 422-437.
Kistler, R.W., Champion, D.E., 2001. Rb–Sr whole-rock and mineral ages, K–Ar, (super 40) Ar/ (super 39) Ar, and U–Pb mineral ages, and strontium, lead, neodymium, and oxygen isotopic compositions for granitic rocks from the Salinian Composite Terrane, California, U. S. Geological Survey, 83, 422-437.
Passchier, C.W., and Trouw, R.A.J., 1996. Microtectonics. Springer-Verlag: Berlin.
Saleeby, J., 2003. Segmentation of the Laramide Slab—evidence from the southern
Sierra Nevada region. Geological Society of America Bulletin, v. 115, no. 6, 655-668.
Vedder, J.G., Howell, D.G., McLean, H., 1982. Stratigraphy, sedimentation, and tectonic accretion of exotic terranes, southern Coast Ranges, California. AAPG Memoir 34, 471–496.